Research on Synchronous Control Method for Suppressing Nonlinear Impulse Perturbation of Photovoltaic Grid-Connected Inverter

ZHAOYAN ZHANG[1], **PEIGUANG WANG**[1], **FANG GAO**[2], **ZHIHENG LIU**[1], **JUNWEI ZHANG**[1], **AND PING JIANG**[1]

[1]College of Electronic Information Engineering, Hebei University, Baoding 071002, China
[2]Institute of Scientific and Technical Information of China, Beijing 100038, China

Corresponding author: Peiguang Wang (pgwang@hbu.edu.cn)

ABSTRACT In this paper, the synchronous control problem of photovoltaic grid-connected inverter with nonlinear impulse perturbation is studied. The mathematical model of photovoltaic grid-connected converter is established by using Kirchhoff's law. The nonlinear impulse perturbation characteristics of grid-connected current are studied and analyzed. Controllers are designed to suppress nonlinear impulse perturbation. The effectiveness of the controller is verified by Lyapunov stability theory. Finally, the simulation design is carried out by simulink in Matlab and the test platform is constructed. In this paper, simulation verification and data comparison are carried out by using various control methods for suppressing nonlinear impulse perturbation of grid-connected currents. Compared with PI controller, PR controller and other controller, the output harmonic content of photovoltaic inverter can be controlled within 1%, which can effectively reduce the harmonic content. The power quality of grid-connected current is improved. The feasibility and effectiveness of the control strategy proposed are verified by simulation and experiments.

INDEX TERMS Nonlinear impulse perturbation, harmonic content, Lyapunov stability, photovoltaic inverter.

I. INTRODUCTION

Energy shortage is a major problem in the world, so it is of great significance to study and develop renewable energy power generation system. Solar energy, as a kind of green energy, has been developed rapidly in the field of renewable energy. With the increasing proportion of photovoltaic power generation capacity in the whole power system, more and more attention has been paid to the influence of the power quality of photovoltaic power generation system on power grid [1]–[3].

The harmonic of power-grid comes from three aspects: the quality of power supply is not high to produce harmonics, the power transmission and distribution system produces harmonics, and the harmonics generated by electrical equipment. Due to the three-phase winding in the manufacture

The associate editor coordinating the review of this manuscript and approving it for publication was Ahmad Elkhateb.

of the generator is difficult to achieve absolute symmetry, the iron core is also difficult to achieve absolute uniformity and some other reasons, the power supply will also produce some harmonics, but generally few. In the power transmission and distribution system, the power transformer mainly produces harmonics. Due to the saturation of the transformer core and the nonlinearity of the magnetization curve, and considering the economy in the design of the transformer, the working magnetic density is selected in the near saturation section of the magnetization curve. In this way, the magnetized current is a spike waveform, so it contains odd harmonics. The wide application of power electronic devices has caused a lot of harmonics to power-grid. For example, the continuous turn on or turn off of power electronic devices in grid-connected inverters of photovoltaic power generation system has a sudden impact on the current. The power-grid harmonic affects the grid-connected control of photovoltaic inverter.

The most commonly used grid-connected current control method of photovoltaic inverter is PI control based on synchronous rotating coordinate system. The algorithm is simple, but the disturbance rejection ability is limited, and the dynamic response speed is slow. When the power network is distorted, additional control algorithms need to be added [4]. On the basis of PI control in rotating coordinate system, a PR(proportional resonant) control method based on static coordinate system is proposed in reference [5]. The algorithm can realize no-error control of power frequency and individual AC harmonic. However, the ability to suppress other harmonics is poor, and the algorithm is relatively complex. In reference [6], the hysteretic control is adopted. The current tracking accuracy is high and the dynamic response is fast, but the switching frequency of the algorithm is not fixed, which makes it difficult to design the filter parameters. In reference [7], repetitive control is used to track periodic signals without static error, but the dynamic performance of the algorithm is poor. In reference [8], [9], the deadbeat control is adopted, which has the advantages of fast response speed and high control precision, but it needs coordinate transformation.

When the photovoltaic inverter is running, the IGBT devices switch quickly and continuously, and the current state suddenly changes or the current step changes. Compared with the whole current process, the duration of these rapid sudden changes is very short, which can be regarded as instantaneous occurrence. This instantaneous abrupt change phenomenon can be described by pulse. And the nonlinear impulse perturbation current, also known as harmonic current, which is a case of harmonic current. The nonlinear impulse perturbation current is common in photovoltaic power generation. Some scholars have studied the influence of nonlinear impulse disturbance on the life of power electronic devices or generator insulation system and the health of grid-connected current in the process of inverter or generator grid-connected [11]. And some scholars have put forward some corresponding control methods [11]–[14]. Based on the detailed analysis of the harmonic mathematical model of grid-side converters, a cross-coupling control strategy for suppressing grid-connected low harmonics current component is proposed in reference [10]. In reference [11], for the pulse problem in nonlinear circuit systems, The idea of modeling is put forward and the corresponding controller is designed. In reference [12], the application of nonlinear factors in power system is introduced according to the characteristics of power system, and the basis principles of various nonlinear power system control technologies is described in detail. The above control methods are to solve the harmonic disturbance control problem from the practical point of view of engineering, but little has been done in theory.

In this paper, the reason of current impulse is analyzed by taking photovoltaic inverter as an example. A feedback synchronization controller is designed based on nonlinear impulse perturbation theory, and the effectiveness of the
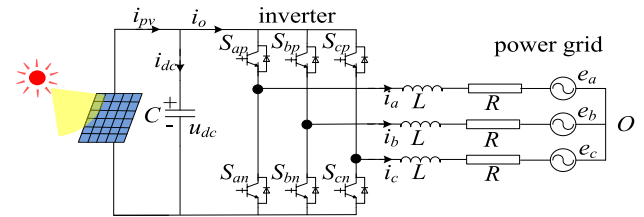

FIGURE 1. Equivalent circuit of photovoltaic grid-connected inverter.

synchronization controller is verified by Lyapunov stability theory. A current impulse perturbation control algorithm is given to suppress the harmonic current into the power grid, and to ensure that the output current of the photovoltaic inverter can be synchronized with the power grid voltage. Compared with PI controller and PR controller, the output harmonic content of photovoltaic inverter can be effectively reduced and the power quality can be improved. Finally, the feasibility and effectiveness of the control strategy proposed in this paper are verified by simulation and experiments.

II. PHOTOVOLTAIC INVERTER MODEL

Photovoltaic grid-connected inverter mainly converts DC current into sinusoidal current which meets the requirements of power grid. The conversion process is completed by turn-on or turn-off of IGBT devices. S_{ap} and S_{bn} switches in Fig.1 are closed, and other switches remain open, A-phase and B-phase current form a closed loop. S_{ap} and S_{bn} switches turn off when A-phase current reaches natural commutation point (the intersection of A-phase current and B-phase current). At the same time, S_{bp} and S_{cn} switches turn on, and other switches remain close, B-phase and C-phase current form a closed loop. When B-phase current reaches the natural commutation point, S_{bp} and S_{cn} switches turn off, S_{cp} and S_{an} switches turn on, and other switches turn off, C-phase and A-phase current form a closed loop current. When C-phase current reaches the natural commutation point, S_{cp} and S_{an} switches turn off. By repeating above process, DC current generated by photovoltaic can be converted into AC current. In the process of fast and continuous switching of IGBT devices, the current state will change abruptly(also known as current step). The duration of these rapid sudden changes is very short compared with the whole process of current movement, which can be considered as instantaneous. This instantaneous sudden change phenomenon can be described by pulse, in which the instantaneous sudden change is called pulse time.

In Fig.1, u_a, u_b, u_c is the three-phase voltage of power grid, i_a, i_b, i_c is the three-phase current of power grid, u_{dc} is DC-side capacitance voltage. And i_{dc} is DC-side capacitance current. R, L are resistance and inductance of shunt reactor of grid-side converter. C is DC side capacitance and i_{pv} is current generated by photovoltaic panels. For convenience, the concept of switching function of grid-side converter is introduced. Assuming that S_m(m = a, b, c) is the switching

function of the m-th phase, S_m can be represented as follows:

$$s_m = \begin{cases} 1 & s_{mp} turnon \\ 0 & s_{mn} turnoff \end{cases} \quad (1)$$

According to the simplified model of grid-connected photovoltaic inverters in Fig.1, the high-frequency mathematical model of grid-connected photovoltaic inverters in three-phase static coordinate system is obtained by Kirchhoff's law [15].

$$\begin{cases} \dfrac{di_a}{dt} = -\dfrac{R}{L}i_a + \dfrac{u_a}{L} - (s_a - \dfrac{s_a + s_b + s_c}{3})u_{dc} \\ \dfrac{di_b}{dt} = -\dfrac{R}{L}i_b + \dfrac{u_b}{L} - (s_b - \dfrac{s_a + s_b + s_c}{3})u_{dc} \\ \dfrac{di_c}{dt} = -\dfrac{R}{L}i_c + \dfrac{u_c}{L} - (s_c - \dfrac{s_a + s_b + s_c}{3})u_{dc} \\ \dfrac{du_{dc}}{dt} = \dfrac{s_a}{C}i_a + \dfrac{s_b}{C}i_b + \dfrac{s_c}{C}i_c - \dfrac{1}{C}i_{pv} \end{cases} \quad (2)$$

Because the switching function S_m(m = a, b, c) in above model contains the high frequency component in switching process, it is difficult to guide the design of the controller in this paper. Assuming that the switching frequency in this model is much higher than the fundamental frequency of power grid, in order to simplify the mathematical model, the high frequency components in the switching function can be neglected. And only the low frequency components in the switching function can be considered, thus the low frequency mathematical model described by duty cycle can be obtained. The switching function is transformed into the corresponding PWM duty cycle by Fourier transform. Its mathematical derivation principle is referred in reference[16]. The mathematical model of low frequency converter described by duty cycle is very suitable for control system analysis and can be directly used in controller design.

In order to facilitate the design of control system, the mathematical model of converter in two-phase stationary coordinate system can be obtained by converting (2) from three-phase stationary coordinate system to two-phase stationary coordinate system [17].

$$\begin{cases} \dfrac{di_\alpha}{dt} = -\dfrac{R}{L}i_\alpha - \dfrac{D_a}{L}u_{dc} + \dfrac{1}{L}u_\alpha \\ \dfrac{di_\beta}{dt} = -\dfrac{R}{L}i_\beta - \dfrac{D_b}{L}u_{dc} + \dfrac{1}{L}u_\beta \\ \dfrac{du_{dc}}{dt} = \dfrac{3}{2C}D_a i_\alpha + \dfrac{3}{2C}D_b i_\beta - \dfrac{1}{C}i_{pv} \end{cases} \quad (3)$$

In this model, u_α, u_β and i_α, i_β represent the voltage and current of α axis and β axis in two-phase static coordinate system, respectively. D_a and D_b are duty cycle of α axis and β axis in static coordinate system. In general, D_a is equal to D_b, and $D_j \in [0, 1](j = a, b)[16]$.

Photovoltaic power plants are generally located in the northwest and northeast of China where solar energy is abundant, and natural conditions are relatively bad. Illumination shows strong non-linearity, non-stationarity, randomness and uncertainty, which aggravates current instability of photovoltaic power plants. With the increasing proportion of photovoltaic power in national grid, its impact on power grid
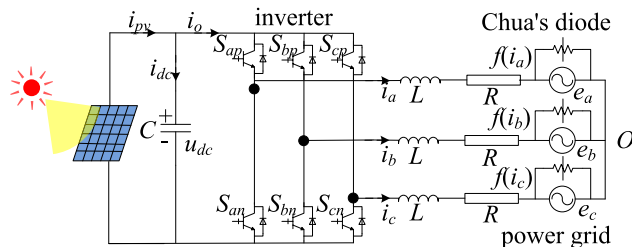

FIGURE 2. Circuit model of PV grid-connected inverter with nonlinear perturbation.

will also increase. Nonlinear perturbation occurs in a large photovoltaic power plant. This kind of nonlinear perturbation will have a great impact on the whole power grid. Therefore, it is necessary to study the complex nonlinear perturbation of current in photovoltaic power generation system with appropriate methods. In this paper, the three-phase voltage source of the power grid is merged into Chua's diode [18]–[20](as shown Fig.2) to simulate nonlinear perturbation of the current of power grid caused by external interference. Chua's diode will not affect the synchronous control of the photovoltaic grid-connected inverter.

Fig.2 is a model of grid-side inverters with nonlinear impulse perturbation. From Fig.2, we can see that $f(i_a)$, $f(i_b)$, $f(i_c)$ is replaced by u_a, u_b, u_c. Then, equation(2) is transformed from three-phase stationary coordinate system to two-phase stationary coordinate system. Combined with (3), the following mathematical models are obtained.

$$\begin{cases} \dfrac{di_\alpha}{dt} = -\dfrac{R}{L}i_\alpha - \dfrac{D_a}{L}u_{dc} + \dfrac{1}{L}f(i_\alpha) \\ \dfrac{di_\beta}{dt} = -\dfrac{R}{L}i_\beta - \dfrac{D_b}{L}u_{dc} + \dfrac{1}{L}f(i_\beta) \\ \dfrac{du_{dc}}{dt} = \dfrac{3}{2C}D_a i_\alpha + \dfrac{3}{2C}D_b i_\beta - \dfrac{1}{C}i_{pv} \end{cases} \quad (4)$$

According to the volt-ampere relationship of Chua's diode, it is as follows:

$$\begin{cases} f(i_\alpha) = u_\alpha = G_a i_\alpha + 0.5(G_a - G_b)[|i_\alpha + I| - |i_\alpha - I|] \\ f(i_\beta) = u_\beta = G_b i_\beta + 0.5(G_a - G_b)[|i_\beta + I| - |i_\beta - I|] \end{cases} \quad (5)$$

In which I, G_a, G_b are typical parameters of Chua's diode. Let:

$$\begin{cases} h(i_\alpha) = \dfrac{1}{L}f(i_\alpha) = G_a \dfrac{i_\alpha}{L} + 0.5(G_a - G_b)\dfrac{[|i_\alpha + I| - |i_\alpha - I|]}{L} \\ h(i_\beta) = \dfrac{1}{L}f(i_\beta) = G_b \dfrac{i_\beta}{L} + 0.5(G_a - G_b)\dfrac{[|i_\beta + I| - |i_\beta - I|]}{L} \end{cases} \quad (6)$$

Let: $m_0 = G_b / L$, $m_1 = G_a / L$, Consider $h(x_1)$ in three sections, as follows:

$$h(i_\alpha) = \begin{cases} m_0 i_\alpha + (m_1 - m_0)I & i_\alpha > I \\ m_1 i_\alpha & |i_\alpha| \leq I \\ m_0 i_\alpha - (m_1 - m_0)I & i_\alpha < -I \end{cases} \quad (7)$$
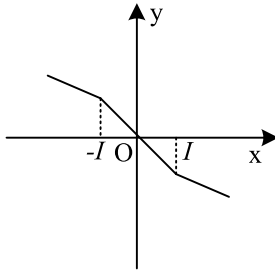
FIGURE 3. Schematic diagram of equation 7.

The schematic diagram of $h(i_\alpha)$ is as follows.From Fig.3, we can see that (5) varies nonlinearly in different regions of x_1.

III. ANALYSIS OF NONLINEAR IMPULSE PERTURBATION AND CONTROLLER DESIGN

A. ANALYSIS OF NONLINEAR IMPULSE PERTURBATION

If for any $x_0 \in R$, there is a domain $U = U(x_0) \subset R$ of x_0 and a constant $l > 0$, such that for any x_1, x_2 has $|h(x_2) - h(x_1)| \leq l |x_2 - x_1|$, then the continuous function $h(x)$ satisfies the local Lipschitz condition on $x \in R$, and the constant l is called the Lipschitz constant.

$$Let : A = \begin{bmatrix} -\dfrac{R}{L} & 0 & -\dfrac{D_a}{L} \\ 0 & -\dfrac{R}{L} & -\dfrac{D_b}{L} \\ \dfrac{3D_a}{2C} & \dfrac{3D_b}{2C} & -\dfrac{i_{pv}}{C} \end{bmatrix} = \begin{bmatrix} -a & 0 & -b \\ 0 & -a & -c \\ d & g & -f \end{bmatrix}$$

Because R, L, C, i_{pv} is a known constant, D_a, $D_b \in [0,1]$ is also a constant.

IGBT devices in grid-connected inverter turn on or turn off continuously, which causes impulse to the current. in order to make the grid-connected current smooth, the impulse control is introduced. For easy derivation, let $x_1 = i_\alpha$, $y_1 = i_\beta$, $z_1 = u_{dc}$. The mathematical model of grid-connected inverter in two-phase static coordinate system is summarized as follows:

$$\begin{cases} \dot{x}_1 = -\dfrac{R}{L}x_1 - \dfrac{D_a}{L}z_1 + \dfrac{1}{L}u_\alpha \\ \dot{y}_1 = -\dfrac{R}{L}y_1 - \dfrac{D_b}{L}z_1 + \dfrac{1}{L}u_\beta \\ \dot{z}_1 = \dfrac{3D_a}{2C}x_1 + \dfrac{3D_b}{2C}y_1 - \dfrac{i_{pv}}{C} \end{cases} \tag{8}$$

Equation(8) is a mathematical model of AC current without impulse perturbation, which is used as a drive system, x_1, y_1, z_1 is the reference value of the controller input. In order to obtain synchronization, the response system model with nonlinear impulse perturbation is constructed as follows:

$$\begin{cases} \dot{x}_2 = -\dfrac{R}{L}x_2 - \dfrac{D_a}{L}z_2 + h(x_2) + u_{c1} + u_{s1} \\ \dot{y}_2 = -\dfrac{R}{L}y_2 - \dfrac{D_b}{L}z_2 + h(y_2) + u_{c2} + u_{s2} \\ \dot{z}_2 = \dfrac{3D_a}{2C}x_2 + \dfrac{3D_b}{2C}y_2 - \dfrac{i_{pv}}{C} + u_{c3} + u_{s3} \end{cases} \tag{9}$$

In which x_2, y_2, z_2 is actual measured value of photovoltaic power generation system. $u_c = \begin{bmatrix} u_{c1} & u_{c2} & u_{c3} \end{bmatrix}^T$ is a synchronous controller. Equation(8) is the drive system and Equation(9) is the response system. the circuit structure of two systems is different, so the structure compensator $u_s = \begin{bmatrix} u_{s1} & u_{s2} & u_{s3} \end{bmatrix}^T$ is added to ensure that the circuit structure of the two systems is the same.

B. CONTROLLER DESIGN

In order to ensure the synchronization between response system (9) and drive system (8), the error variables are defined for the drive system (8) and the response system (9):

$$e = \begin{bmatrix} e_1 \\ e_2 \\ e_3 \end{bmatrix} = \begin{bmatrix} x_2 & -x_1 \\ y_2 & -y_1 \\ z_2 & -z_1 \end{bmatrix} \tag{10}$$

According to (9), the whole controller u_{t_c} is composed of synchronous controller u_c and compensator u_s, as follows:

$$u_{t\_c} = u_c + u_s \tag{11}$$

The response system (9) and the drive system (8) are synchronized under the whole controller u_{t_c}. And the synchronous controller u_c is as follows:

$$u_c = \begin{bmatrix} u_{c1} \\ u_{c2} \\ u_{u3} \end{bmatrix} = \begin{bmatrix} k_{p1}e_1 + k_{i1} \int\limits_{\tau=0}^{t} e_1(\tau)d\tau \\ k_{p2}e_2 + k_{i2} \int\limits_{\tau=0}^{t} e_2(\tau)d\tau \\ k_{p3}e_3 + k_{i3} \int\limits_{\tau=0}^{t} e_3(\tau)d\tau \end{bmatrix} \tag{12}$$

In which k_{p_1}, k_{p_2}, k_{p_3} is proportional control gain coefficient. k_{i_1}, k_{i_2}, k_{i_3} is integral control gain coefficient. τ is calculus variable of integration.

There is a capacitance on the DC side of the photovoltaic inverter, which can eliminate the disturbance, so the pulse disturbance of the capacitor voltage can be ignored. The compensator does not compensate the capacitor voltage, but only the output current of the inverter. The compensator is as follows.

$$\begin{cases} u_{s1} = \dfrac{u_\alpha}{L} - h(x_1) \\ u_{s2} = \dfrac{u_\beta}{L} - h(y_1) \\ u_{s3} = 0 \end{cases} \tag{13}$$

Use (9) and (8) to make a difference, and bring (13) into equation, then the error system model can be obtained:

$$\begin{cases} \dot{e}_1 = -\dfrac{R}{L}e_1 - \dfrac{D_a}{L}e_3 + h(x_2) - h(x_1) + u_{c1} \\ \dot{e}_2 = -\dfrac{R}{L}e_2 - \dfrac{D_b}{L}e_3 + h(y_2) - h(y_1) + u_{c2} \\ \dot{e}_3 = \dfrac{3D_a}{2C}e_1 + \dfrac{3D_b}{2C}e_2 - \dfrac{i_{pv}}{C}e_2 + u_{c3} \end{cases} \tag{14}$$

Under the control of controller, if $e_1 = 0$, $e_2 = 0$, $e_3 = 0$, then the response system (9) with nonlinear impulse

perturbation will approach the unperturbed drive system (8), that is, the nonlinear impulse peturbation will be suppressed effectively.

Taking Lyapunov function $V = (e_1^2 + e_2^2 + e_3^2)/2$, and knowing from reference [21]–[22] that nonlinear function $h(x_1)$ satisfies local Lipschitz condition, there are:

$$
\begin{aligned}
\dot{V} &= e_1\dot{e}_1 + e_2\dot{e}_2 + e_3\dot{e}_3 \\
&= e_1(-\frac{R}{L}e_1 - \frac{D_\alpha}{L}e_3 + h(x_2) - h(x_1) + u_{c1}) \\
&\quad + e_2(-\frac{R}{L}e_2 - \frac{D_\beta}{L}e_3 + h(y_2) + u_{c2}) \\
&\quad + e_3(\frac{3D_a}{2C}e_1 + \frac{3D_\beta}{2C}e_2 - \frac{1}{R_1 C}e_2 + u_{c3}) \\
&= -ae_1^2 + (d-b)e_1 e_3 + [h(x_2) - h(x_1)]e_1 - u_{c1}e_1 - ae_2^2 \\
&\quad + (g-c)e_2 e_3 + [h(y_2) - h(y_1)]e_2 - u_{c2}e_2 - fe_3^2 - u_{c3}e_3
\end{aligned}
$$
$$(15)$$

According to the lagrange mean value theorem: $f(x_2) - f(x_1) = f'(\xi)|x_2 - x_1|$, takes $l_1, l_2 = \max\{h'(\xi)\}$, there is:

$$
\begin{cases}
h(x_2) - h(x_1) \le l_1 e_1 \\
h(y_2) - h(y_1) \le l_2 e_2
\end{cases}
\tag{16}
$$

Substituting (16) into (15), we can obtain:

$$
\begin{aligned}
\dot{V} &\le -ae_1^2 + (d-b)e_1 e_3 + l_1 e_1^2 - u_{c1}e_1 - ae_2^2 \\
&\quad + (g-c)e_2 e_3 + l_2 e_2^2 - u_{c2}e_2 - fe_3^2 - u_{c3}e_3 \\
&\le -ae_1^2 + \frac{(d-b)}{2}(e_1^2 + e_3^2) + l_1 e_1^2 - u_{c1}e_1 - ae_2^2 \\
&\quad + \frac{(g-c)}{2}(e_2^2 + e_3^2) + l_2 e_2^2 - u_{c2}e_2 - fe_3^2 - u_{c3}e_3
\end{aligned}
\tag{17}
$$

Substituting (12) into (17), we can obtain:

$$
\begin{aligned}
\dot{V} &\le -ae_1^2 + \frac{d-b}{2}(e_1^2 + e_3^2) + l_1 e_1^2 - k_{p1}e_1^2 - k_{i1}e_1 \int_{\tau=0}^{t} e_1(\tau)d\tau \\
&\quad - ae_2^2 + \frac{g-c}{2}(e_2^2 + e_3^2) + l_2 e_2^2 - k_{p2}e_2^2 - k_{i2}e_2 \int_{\tau=0}^{t} e_2(\tau)d\tau \\
&\quad - fe_3^2 - k_{p3}e_3^2 - k_{i3}e_3 \int_{\tau=0}^{t} e_3(\tau)d\tau \\
&\le -ae_1^2 + \frac{d-b}{2}(e_1^2 + e_3^2) + l_1 e_1^2 - k_{p1}e_1^2 - \frac{k_{i1}}{2}e_1^2 \\
&\quad - ae_2^2 + \frac{g-c}{2}(e_2^2 + e_3^2) + l_2 e_2^2 - k_{p2}e_2^2 - \frac{k_{i2}}{2}e_2^2 \\
&\quad - fe_3^2 - k_{p3}e_3^2 - \frac{k_{i3}}{2}e_3^2 \\
&= -[(a + k_{p1} + \frac{1}{2}b - \frac{1}{2}d - l_1 + \frac{k_{i1}}{2})e_1^2 \\
&\quad + (a + k_{p2} + \frac{1}{2}c - \frac{1}{2}g - l_2 + \frac{k_{i2}}{2})e_2^2 \\
&\quad + (k_3 + f + \frac{1}{2}b + \frac{1}{2}c - \frac{1}{2}d - \frac{1}{2}g + \frac{k_{i3}}{2})e_3^2]
\end{aligned}
\tag{18}
$$

Let λ is as follows:

$$
\lambda = \min \begin{Bmatrix} 2a + 2k_{p1} + b - 2l_1 - d + k_{i1} \\ 2a + 2k_{p2} + c - 2l_2 - g + k_{i2} \\ 2k_{p3} + 2f + b + c - d - g + k_{i3} \end{Bmatrix} > 0
\tag{19}
$$

According to (18) and (19), we can obtain:

$$
\dot{V} \le -\lambda V = -\frac{\lambda}{2}(e_1^2 + e_2^2 + e_3^2)
\tag{20}
$$

According to (20), $\dot{V}/V \le -\lambda$ is obtained. Integrating two sides of the inequality from $0 \to t$, $V(t) \le e^{-\lambda t}$ can be obtained. When $t \to \infty, V(t)$ is 0, so $e_1 \to 0$, $e_2 \to 0$, $e_3 \to 0$. The response system (9) and the drive system (8) are synchronized, that is, the nonlinear impulse peturbation will be suppressed.

In summary, l_1, l_2 is the specific value, and a, b, c, d, f, g as follows:

$$
A = \begin{bmatrix} -\dfrac{R}{L} & 0 & -\dfrac{D_a}{L} \\ 0 & -\dfrac{R}{L} & -\dfrac{D_b}{L} \\ \dfrac{3D_a}{2C} & \dfrac{3D_b}{2C} & -\dfrac{i_{pv}}{C} \end{bmatrix} = \begin{bmatrix} -a & 0 & -b \\ 0 & -a & -c \\ d & g & -f \end{bmatrix}
$$

Based on the above derivation, the values of controller k_{p_1}, k_{p_2}, k_{p_3}, k_{i_1}, k_{i_2}, k_{i_3} can be obtained.

PI control is the most commonly used control method for photovoltaic grid-connected inverter to track the power-grid current, but its ability to suppress low-order harmonics is weak. The above derivation and verification process can be concluded that the whole controller u_{t_c} is composed of PI controller u_c and a feedforward compensator u_s, which is used to compensate the nonlinear power-grid voltage perturbation, as shown in (13). In this paper, an additional compensation mechanism is added to improve the performance of the grid-connected current. The combined control method can reduce the steady-state error of the system and has good robustness. The logic block diagram of the controller can be obtained from (12), (13), (14), (19) and (29). Fig.4 is a Block diagram of current impulsive perturbation control model for grid-connected inverters.

As can be seen from Fig.4, the three phase grid-connected current is transformed by clarke to get the currents of α/β coordinate system, and the three phase power-grid voltage is transformed by clarke to get the voltage of α/β coordinate system. u_{dc}^* is the reference value of DC circuit voltage. According to (14), the error value is obtained by subtracting the reference value u_{dc}^* from the actual value u_{dc} (or $u_{dc} - \dfrac{i_{pv}}{C}$ in β axis), and the current reference value i_α^*/i_β^* in α/β coordinate system can be obtained through the voltage PI controller. The voltage PI controller mainly keeps DC voltage u_{dc} constant and has good dynamic response by controlling current i_α and i_β, as shown in the third item of (14). And the error value is obtained by subtracting the reference value i_α^*/i_β^* from the actual value i_α/i_β, and the reference voltage control value $u_{ctr\_\alpha}^*/u_{ctr\_\beta}^*$ can be obtained through the current
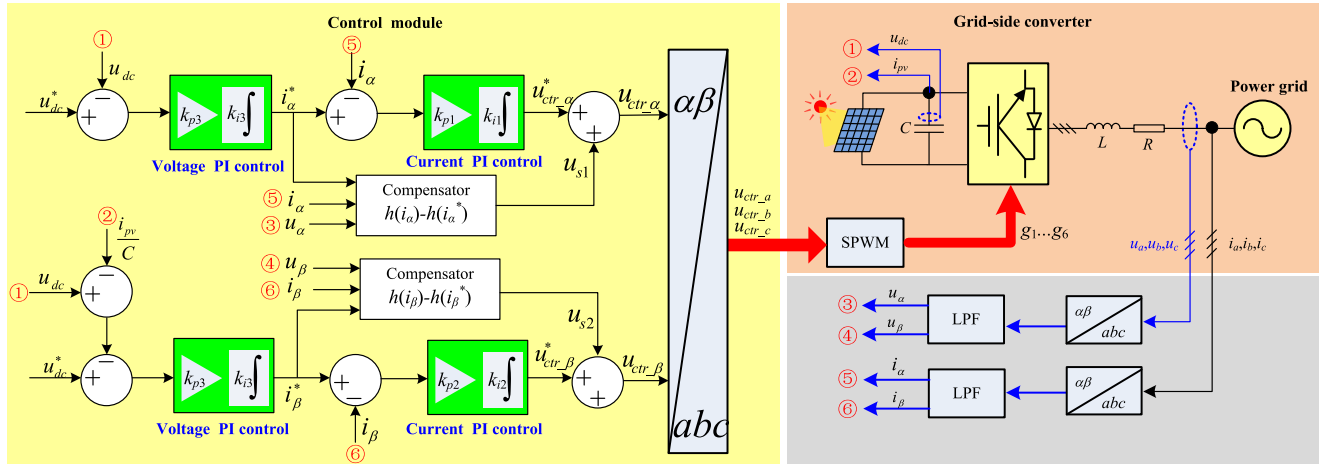
FIGURE 4. Block diagram of current impulsive perturbation control model for grid-connected inverters.

PI controller. The current PI controller mainly controls the output current, as shown in the first and second items of (14). The actual voltage control value $u_{ctrl\_\alpha}/u_{ctrl\_\beta}$ is that the reference voltage control value $u^*_{ctr\_\alpha}/u^*_{ctr\_\beta}$ plus compensation value u_{s_1}/u_{s_2}. Compensation control is mainly used to suppress low-order harmonics and improve the performance of grid-connected current. The actual voltage control value $u_{ctrl\_\alpha}/u_{ctrl\_\beta}$ is transformed to three phase control voltage vaule $u_{ctrl\_a}/u_{ctrl\_b}/u_{ctrl\_c}$ of abc coordinate system by inverse Clarke transformation. The three phase control voltage vaules are sent to the SPWM block as a modulation wave to generate six-channel logic signal of driving IGB switch.

IV. SIMULATION AND EXPERIMENTAL VERIFICATION
A. SIMULATION VERIFICATION
1) SIMULATION VERIFICATION WITH PROPOSED CONTROLLER
In order to verify the correctness and effectiveness of the proposed control strategy for suppressing nonlinear current perturbation of grid-connected converter, a simulation model of photovoltaic grid-connected power generation system is built in Matlab/Simulink software, and the simulation research and analysis are carried out. The simulation model parameters are as follows. The inlet reactor resistance R is 0.52Ω, the inlet reactor inductance L is 10mH, the DC side capacitance C is 2200μF, the DC side voltage is 400V, the switching frequency is 10kHz, Duty cycle is 0.2. The parameter l_1 equals l_2, which is 0.002. The specific values of a, b, c, d, f, g can be calculated, and the value of control perturbation of the controller u_{c_1}, u_{c_2}, u_{c_3} can be calculated.

Fig.5 shows AC current waveform with nonlinear impulse perturbation. The continuous turn on or turn off of IGBT devices in grid-connected inverters has a sudden impact on the current.

Fig.6 is comparison of A phase standard reference sinusoidal current and regulated nonlinear impulse perturbation AC current. From Fig.6, it can be seen that the
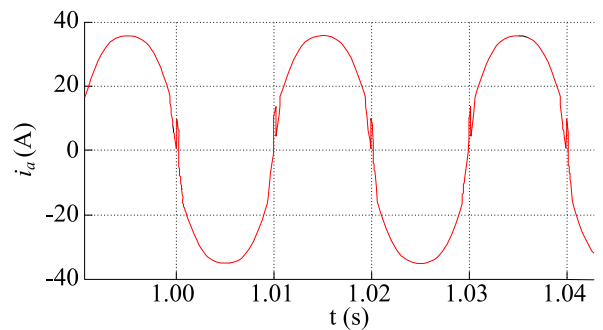

FIGURE 5. AC Current with nonlinear impulse pertrubation.

AC waveform obtained by the proposed controller after the sinusoidal current is disturbed by a nonlinear impulse perturbation is exactly the same as amplitude and phase angle of standard reference sinusoidal current.

Fig.7 is adjustment error curve. From Fig.7, it can be seen that the error converges asymptotically to 0 under the action of proposed controller, that is, the AC current with nonlinear impulse perturbation approaches to the AC current without nonlinear impulse perturbation. It is verified that the proposed controller can effectively suppress the AC current with nonlinear impulse perturbation, Such that synchronization is achieved between AC current with nonlinear impulse perturbation and standard reference AC current.

Fig.8 shows power-grid voltage and the output current of the grid-side inverter under proposed controller. It can be seen from Fig.8 that the grid-connected current waveform is smooth, the distortion at the peak value is small, and the current peak burr is reduced, and the grid-connected current waveform is better.

2) SIMULATION COMPARISON WITH PI CONTROLLER, PR CONTROLLER AND OTHER CONTROLLERS
In order to highlight the effectiveness of the proposed method for harmonic suppression, the simulation results of proposed method are compared with PI controller, PR controller and
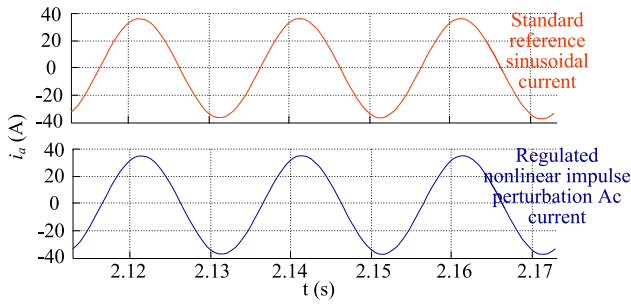
FIGURE 6. Comparison of a phase standard reference sinusoidal current and regulated nonlinear impluse perturbation AC current.
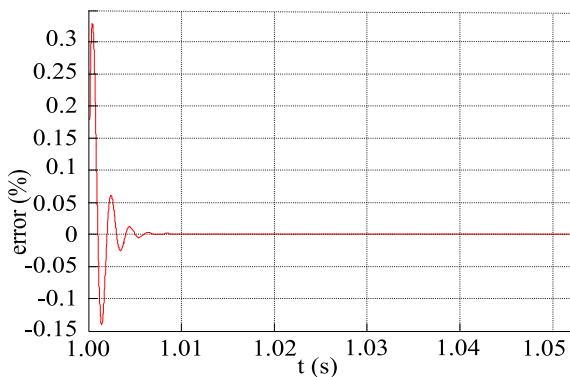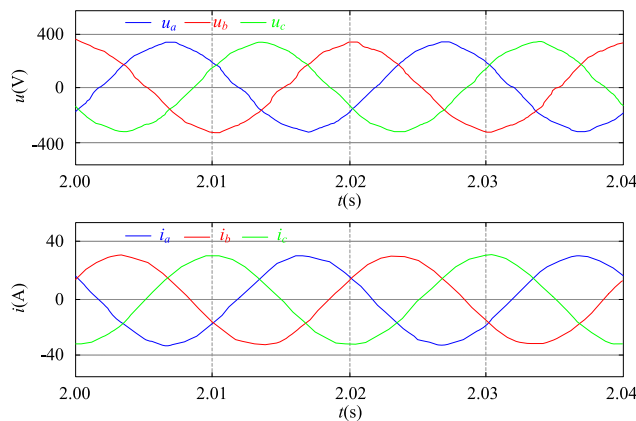

FIGURE 7. Adjustment error curve.

FIGURE 8. Power grid voltage and the output current of the grid-side converter under the proposed controller.

other controllers. The simulation model is built on Simulink platform, the system switching frequency is 10kHz, Under the same conditions, the simulation experiments are carried out on the PI controller, the PR controller, proposed controller and other controllers in this paper.

As shown in Fig.9, when the PI controller is used, the total harmonic content is 4.31%, and the odd harmonic content is mainly 5th and 7th harmonics. And 5th harmonic content is 2.86% and 7th harmonic content is 1.35%. The PI controller can not effectively suppress the lower harmonics content of the grid-connected current. As shown in Fig.10, when the PR controller is used, the 5th and 7th harmonics can be
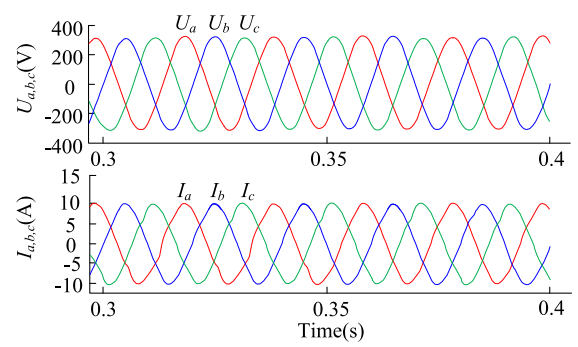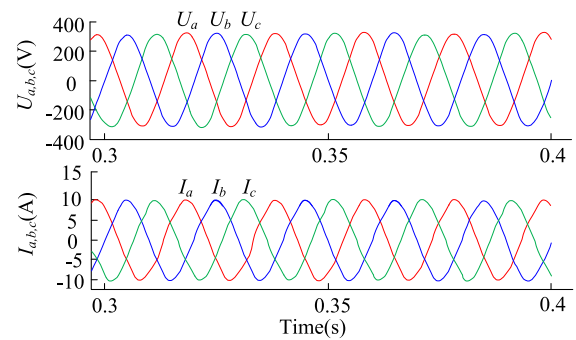

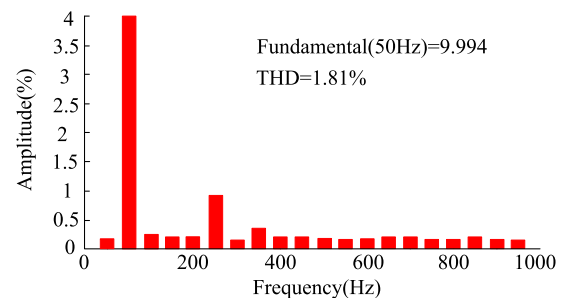(a) Simulation results of grid-connected current under PI control
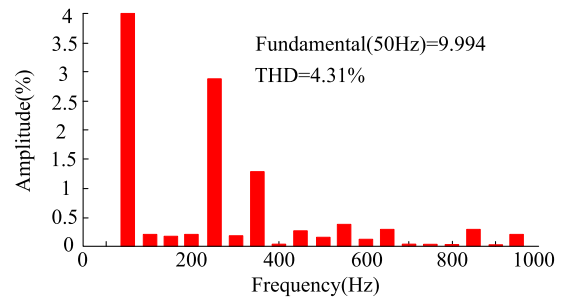
(b) Harmonic analysis of grid-connected current under PI control

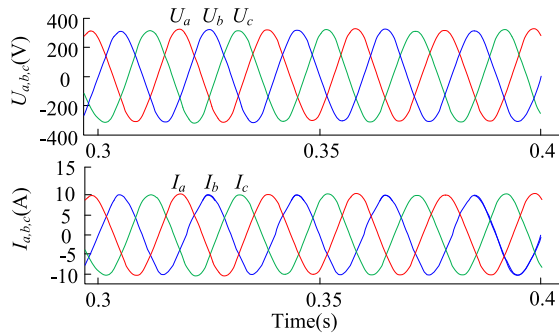**FIGURE 9.** Simulation results of grid-connected currend and harmonic analysis under PI control.

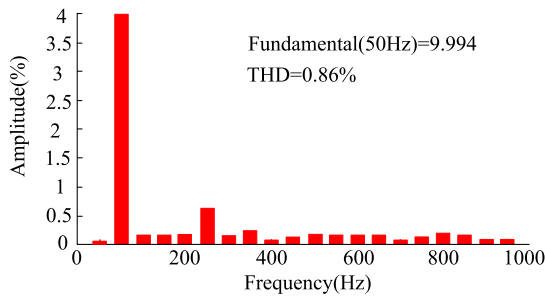(a) Simulation results of grid-connected current under PR control

(b) Harmonic analysis of grid-connected current under PR control

FIGURE 10. Simulation results of grid-connected currend and harmonic analysis under PR control.

suppressed. The total harmonic content is 1.81%. The 5th harmonic content is reduced to 0.90%, and the 7th harmonic content is reduced to 0.35%.

(a) Simulation results of grid-connected current under proposed control

Fundamental(50Hz)=9.994
THD=0.86%

(b) Harmonic analysis of grid-connected current under proposed control

FIGURE 11. Simulation results of grid-connected currend and harmonic analysis under proposed control.

TABLE 1. Comparison of grid-connected current harmonic contents under various controllers.

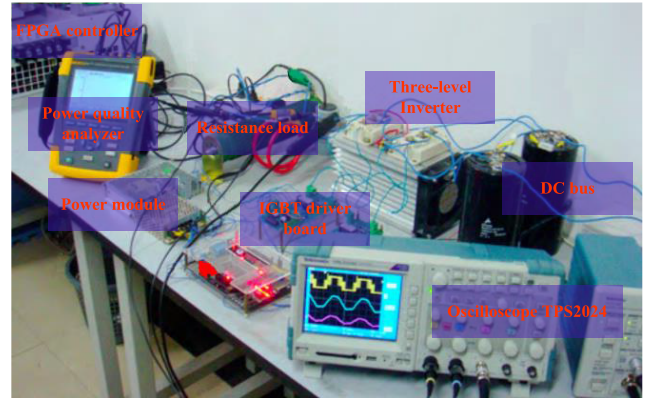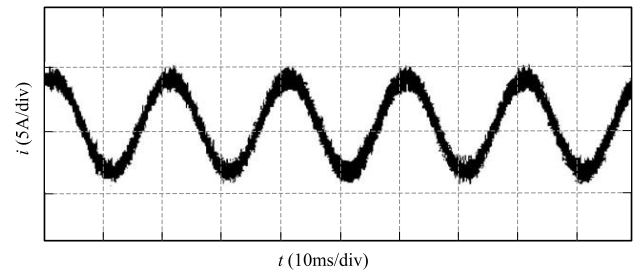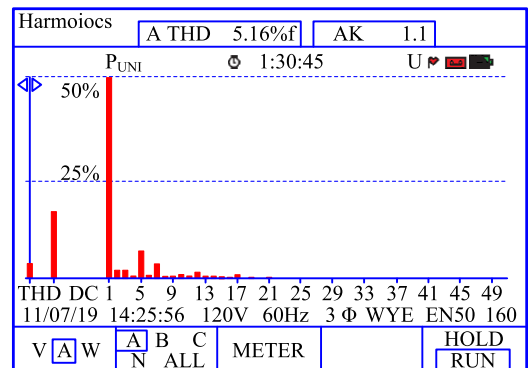| Control method	total harmonic content(%)	5th harmonic content(%)	7th harmonic content(%)
PI	4.31	2.86	1.35
PR	1.81	0.9	0.35
RC	3.38	2.06	1.12
PI+PCI	1.54	0.87	0.59
Proposed control	0.86	0.58	0.23

FIGURE 12. Experimental platform of three-level inverter.

(a) Experimental results of grid-connected current under PI control

(b) Harmonic analysis of grid-connected current under PI control

FIGURE 13. Experimental results of grid-connected current waveforms and harmonic analysis under PI control.

In addition, the repetitive control(RC) method based on internal model principle, PI control + proportional complex integral (PCI) control method(PI+PCI) are simulated and verified, and grid-connected current harmonic analysis is carried out. Under the RC controller, the total harmonic content is 3.38%, and 5th harmonic content is 2.06% and 7th harmonic content is 1.12%. Under the PI+PCI controller, the total harmonic content is 1.54%, and 5th harmonic content is 0.87% and 7th harmonic content is 0.59%.

Compared with the PI controller, the PR controller and other controllers, the proposed controller can effectively reduce the harmonic content. As shown in Fig.11, when proposed controller is used, the total harmonic content is 0.86%. The 5th harmonic content is reduced to 0.58%, and the 7th harmonic content is reduced to 0.23%. The higher harmonic is lower than that of other controllers. The total harmonic content is much lower than that of other controllers. The simulation results show that the nonlinear impulse perturbation control method can effectively suppress the harmonics of grid-connected current. Table. 1 shows the comparison of grid-connected current harmonic contents under various controllers.

B. EXPERIMENTAL VERIFICATION

In order to verify the effectiveness of proposed control strategy in this paper, an experimental platform is built, as shown in Fig.12. MDO3034 or agilent oscilloscope and FLUKE435 power analyzer were used for measurement.

The core processor of the experimental platform is the TMS320F28335 DSP controller, and the working frequency of the DSP is 150 MHz. The main circuit adopts three-phase
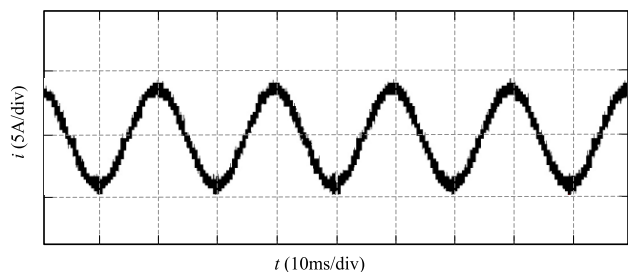
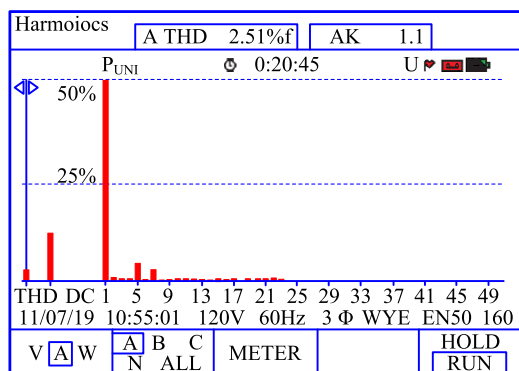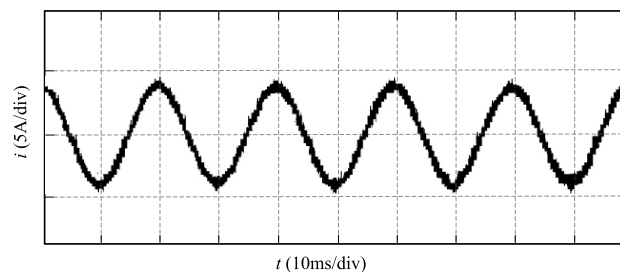(a) Experimental results of grid-connected current under PR control

(b) Harmonic analysis of grid-connected current under PR control

FIGURE 14. Experimental results of grid-connected current waveforms and harmonic analysis under PR control.

bridge topology, and the switching frequency of the system is 10 kHz, the inlet reactor inductance L is 5mH, the DC side capacitance C is 1000μF. The DC bus voltage is 320 V, and AC network side is connected to power-grid with a three-phase transformer at 1:2.

Fig.13 shows the current waveform and harmonic content of A-phase grid-connected current under PI control. In Fig.13 (a), it can be seen that there are many sharp burrs in grid-connected current under PI control, the current waveform is rough and not smooth, and the distortion at the peak value is large. The data of the power analyzer is shown in Fig.13 (b). Through the data of the power analyzer, it can be seen that current harmonic content is 5.16%, and there are large lower harmonics in grid-connected current, in which the odd harmonic content is mainly 5th and 7th harmonics. Under the same experimental conditions, the grid-connected operation of photovoltaic inverter is controlled by PR control algorithm, and the grid-connected current waveform is shown in Fig.14 (a). Compared with PI control algorithm, it can be seen that grid-connected current is smoother under the PR control algorithm. The peak and peak distortion is small, and the burr of current peak is reduced, and the waveform of grid-connected current is better. The data of the power analyzer is shown in Fig.14 (b), the harmonic content of the grid-connected current is 2.51%, and the total harmonic content is reduced from 5.16% to 2.51%, of which the 5th and 7th harmonic content is reduced.

Under the RC control method, the total current harmonic content is 3.17%. And the total current harmonic content is 1.68% under the PI+PCI control method.

(a) Experimental results of grid-connected current under proposed control
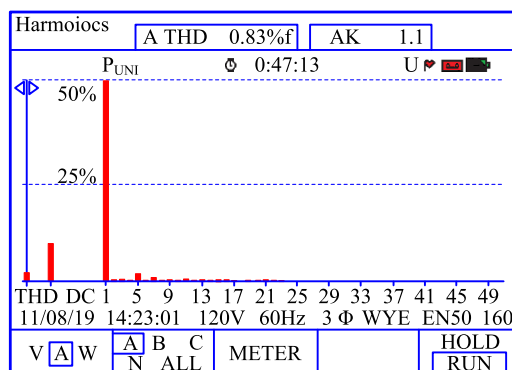
(b) Harmonic analysis of grid-connected current under proposed control

FIGURE 15. Experimental results of grid-connected current waveforms and harmonic analysis under proposed control.

When proposed control algorithm is used, the grid-connected current waveform is shown in Fig.15 (a). It can be seen that the grid-connected current waveform is smooth, the distortion at the peak value is small, and the current peak is greatly reduced, and the grid-connected current waveform is better. The data of the power analyzer is shown in Fig.15 (b), the harmonic content of the grid-connected current is 0.83%. The total harmonic content is less than 1%, and the 5th and 7th harmonic content is greatly reduced.

The experimental results show that compared with PI controller and PR controller, the harmonic content of grid-connected current is greatly reduced. And the harmonic content can be controlled within 1%, which can effectively reduce the harmonic content. The power quality of grid-connected current is improved.

V. CONCLUSION

Nonlinear impulse perturbation of grid-connected current of photovoltaic inverter will have a great impact on power grid, so it is very necessary to study complex nonlinear perturbation phenomenon of photovoltaic system current. In this paper, firstly, the mathematical model of photovoltaic grid-connected converter is established by using Kirchhoff's law, then nonlinear impulse perturbation characteristics of grid-connected current are studied and analyzed. On the basis of this, nonlinear impulse perturbation controllers are designed to suppress nonlinear impulse perturbation. Based on Lyapunov stability theory, the effectiveness

of synchronous controller is proved. Finally, the simulation design is carried out by simulink in Matlab and the test platform is constructed. The feasibility and effectiveness of the control strategy proposed are verified by simulation and experiments. Compared with PI controller, PR controller, and other controller, the harmonic content of grid-connected current is greatly reduced under proposed controller. And the harmonic content can be controlled within 1%, which can effectively reduce the harmonic content. The power quality of grid-connected current is improved.

REFERENCES

[1] E. Serban, M. Ordonez, and C. Pondiche, "DC-bus voltage range extension in 1500 V photovoltaic inverters," *IEEE J. Emerg. Sel. Topics Power Electron.*, vol. 3, no. 4, pp. 901–917, Dec. 2015.

[2] E. Serban, F. Paz, and M. Ordonez, "Improved PV inverter operating range using a miniboost," *IEEE Trans. Power Electron.*, vol. 32, no. 11, pp. 8470–8485, Nov. 2017.

[3] D.-T. Do and M.-K. Nguyen, "Three-level quasi-switched boost T-type inverter: Analysis, PWM control, and verification," *IEEE Trans. Ind. Electron.*, vol. 65, no. 10, pp. 8320–8329, Oct. 2018.

[4] M. Reyes, P. Rodriguez, S. Vazquez, A. Luna, R. Teodorescu, and J. M. Carrasco, "Enhanced decoupled double synchronous reference frame current controller for unbalanced grid-voltage conditions," *IEEE Trans. Power Electron.*, vol. 27, no. 9, pp. 3934–3943, Sep. 2012.

[5] D. Zmood and D. Holmes, "Stationary frame current regulation of PWM inverters with zero steady-state error," *IEEE Trans. Power Electron.*, vol. 18, no. 3, pp. 814–822, May 2003.

[6] L. Quanwei, D. Yan, and H. Yihua, "Current prediction and virtual over-sampling based digital hysteresis control," *Trans. China Electrotech. Soc.*, vol. 29, no. 10, pp. 127–133, 2014.

[7] J. Yaoqin, Z. Minglin, and F. Yong, "State feedback based repetitive control for single-phase inverter," *Trans. China Electrotech. Soc.*, vol. 29, no. 6, pp. 57–63, 2014.

[8] M. Pichan, H. Rastegar, and M. Monfared, "Deadbeat control of the stand-alone four-leg inverter considering the effect of the neutral line inductor," *IEEE Trans. Ind. Electron.*, vol. 64, no. 4, pp. 2592–2601, Apr. 2017.

[9] W. Jiang, X. Ding, Y. Ni, J. Wang, L. Wang, and W. Ma, "An improved deadbeat control for a three-phase three-line active power filter with current-tracking error compensation," *IEEE Trans. Power Electron.*, vol. 33, no. 3, pp. 2061–2072, Mar. 2018.

[10] L. Yu, "Effects of converter pulse volage on insulation life of doubly-fed wind generators," *Power Equip.*, vol. 28, no. 3, pp. 186–188, Mar. 2014.

[11] L. Sainz, J. J. Mesas, R. Teodorescu, and P. Rodriguez, "Deterministic and stochastic study of wind farm harmonic currents," *IEEE Trans. Energy Convers.*, vol. 25, no. 4, pp. 1071–1080, Dec. 2010.

[12] Y. Jun, X. Xianfeng, C. Xiyin, and L. Yong, "Harmonic currents suppression for full size power grid-connection converter used for wind power generation," *Proc. CSEE*, vol. 32, no. 16, pp. 17–25, Jun. 2012.

[13] H. Yang, P. Li, Y. Xia, and C. Yan, "Double-loop stability for high frequency networked control systems subject to actuator saturation," *IEEE Trans. Cybern.*, vol. 49, no. 4, pp. 1454–1462, Apr. 2019.

[14] X.-H. Chang and Y.-M. Wang, "Peak-to-peak filtering for networked non-linear DC motor systems with quantization," *IEEE Trans. Ind. Informat.*, vol. 14, no. 12, pp. 5378–5388, Dec. 2018.

[15] Z. Yang and D. Xu, "Stability analysis and design of impulsive control systems with time delay," *IEEE Trans. Autom. Control*, vol. 52, no. 8, pp. 1448–1454, Aug. 2007.

[16] L. Dong and Y. Takeuchi, "Impulsive control of multiple Lotka-Volterra systems," *Nonlinear Anal., Real World Appl.*, vol. 14, no. 2, pp. 1144–1154, Feb. 2013.

[17] S. Li, J. Zhang, and W. Tang, "Robust H∞ control for impulsive switched complex delayed networks," *Math. Comput. Model.*, vol. 56, nos. 11–12, pp. 257–267, Dec. 2012.

[18] C. Yuan, "Robust H∞ consensus for multi-agent systems with time-varying input delay using dynamic IQCs," in *Proc. Amer. Control Conf. (ACC)*, vol. 2017, May 2017, pp. 930–935.

[19] M. Yang, Y.-W. Wang, J.-W. Xiao, and Y. Huang, "Robust synchronization of singular complex switched networks with parametric uncertainties and unknown coupling topologies via impulsive control," *Commun. Nonlinear Sci. Numer. Simul.*, vol. 17, no. 11, pp. 4404–4416, Nov. 2012.

[20] H. Geng, C. Liu, and G. Yang, "LVRT capability of DFIG-based WECS under asymmetrical grid fault condition," *IEEE Trans. Ind. Electron.*, vol. 60, no. 6, pp. 2495–2509, Jun. 2013.

[21] R. Rakkiyappan, G. Velmurugan, and J. Cao, "Finite-time stability analysis of fractional-order complex-valued memristor-based neural networks with time delays," *Nonlinear Dyn.*, vol. 78, no. 4, pp. 2823–2836, Dec. 2014.

[22] S. Zanfang, P. Imkeller, and T. Shenzhang, "Global flows for stochastic differential equations without global Lipschitz conditions," *Math. Statist. Online*, vol. 35, no. 1, pp. 180–205, Jan. 2007.

[23] Y. Sun and J. Cao, "Adaptive synchronization between two different noise-perturbed chaotic systems with fully unknown parameters," *Phys. A, Stat. Mech. Appl.*, vol. 376, pp. 253–265, Mar. 2007.

[24] R. Rakkiyappan, A. Chandrasekar, and G. Petchiammal, "Non-fragile robust synchronization for Markovian jumping chaotic neural networks of neutral-type with randomly occurring uncertainties and mode-dependent time-varying delays," *ISA Trans.*, vol. 53, no. 6, pp. 1760–1770, Nov. 2014.

[25] H. Wang, S. Duan, C. Li, L. Wang, and T. Huang, "Stability of impulsive delayed linear differential systems with delayed impulses," *J. Franklin Inst.*, vol. 352, no. 8, pp. 3044–3068, Aug. 2015.

[26] G. Velmurugan, R. Rakkiyappan, and J. Cao, "Further analysis of global μ-stability of complex-valued neural networks with unbounded time-varying delays," *Neural Netw.*, vol. 67, pp. 14–27, Jul. 2015.

[27] S. Wen, Z. Zeng, T. Huang, and C. Li, "Passivity and passification of stochastic impulsive memristor-based piecewise linear system with mixed delays," *Int. J. Robust Nonlinear Control*, vol. 25, no. 4, pp. 610–624, Mar. 2015.

[28] X. Yang and J. Cao, "Hybrid adaptive and impulsive synchronization of uncertain complex networks with delays and general uncertain perturbations," *Appl. Math. Comput.*, vol. 227, pp. 480–493, Jan. 2014.

[29] C. Briat, "Stability analysis and control of a class of LPV systems with piecewise constant parameters," *Syst. Control Lett.*, vol. 82, pp. 10–17, Aug. 2015.

[30] Z. Zhang and P. Wang, "Research and implementation of natural sampling spwm digital method for three-level inverter of photovoltaic power generation system based on FPGA," *IEEE Access*, vol. 7, pp. 114449–114458, 2019.
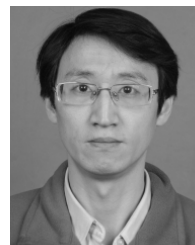
ZHAOYAN ZHANG received the B.S. degree in computer science and technology from the College of Mathematics and Computer Science, Hebei University, Baoding, China, in 2003, and the M.S. and Ph.D. degrees in control theory and control engineering from North China Electric Power University, Baoding, in 2011 and 2017, respectively.

From 2016 to 2018, he was a Senior Engineer with Baoding SinoSimu Technology Company, Ltd., Baoding. Since 2018, he has been an Associate Professor with the College of Electronic Information Engineering, Hebei University, where he is currently a Postdoctoral Researcher. His research interest includes new energy power generation technology, power electronic converter technology, and motor speed regulation.

PEIGUANG WANG received the Ph.D. degree in applied mathematics from the Beijing Institute of Technology, Beijing, China, in 2000. He has been a Visiting Professor with the Department of Mathematics and Statistics, Curtin University, Australia, many times for different durations, from 2002 to 2015. He is currently a Professor with the College of Electronic Information Engineering, Hebei University, China. His research interests include nonlinear analysis and numerical simulation.

FANG GAO received the Ph.D. degree in control theory and control engineering from the College of Control and Computer Engineering, North China Electric Power University, Beijing, China, in 2013, and the M.S. degree in communication and information system from the College of Electronic Information Engineering, Hebei University, Baoding, in 2005.

From 2008 to 2013, she was a Lecturer with the College of Electronic Information Engineering, Hebei University. From 2013 to 2015, she conducted Postdoctoral Research in information science with the Institute of Scientific and Technical Information of China, Beijing, where she is currently an Assistant Professor. Her research interests include intelligent optimization theory and algorithm, and science and technology policy and strategy.

JUNWEI ZHANG was born in Baoding, Hebei, China, in 1974. He received the B.S. degree in mechanical design and manufacturing from the Agriculture of Hebei University, China, in 1996, and the M.S. and Ph.D. degrees in mechanical design theory from North China Electric Power University, China, in 2003 and 2011, respectively.

From 2005 to 2011, he was a Research Assistant with the Institute of North China Electric Power University Simulation Control Technology Engineering Study Center. Since 2011, he has been an Assistant Professor with the College of Electronic Information Engineering, Hebei University. His research interest includes the application of artificial intelligence on engineering technology, power conversion technique, energy-saving technology of large motor, and electric drive.

ZHIHENG LIU received the M.S. degree in electric machines and electric apparatus from the Taiyuan University of Technology, Taiyuan, China, in 2011, and the Ph.D. degree in electric machines and electric apparatus from the Dalian University of Technology, Dalian, China, in 2017.

He is currently a Postdoctoral Fellow in photoelectric engineering with the Key Laboratory of Opto-electronic Information Technology, Ministry of Education, Tianjin University, Tianjin, China, and a Lecturer with the College of Electronic Information Engineering, Hebei University, Baoding, China. His current research activities are intelligent high-voltage apparatus and intelligent testing technology, and emphasis on electrical equipment on-line detection and insulation diagnosis, advanced fiber inspection technology, and electromagnetic immunity testing technology.

PING JIANG was born in Yu Xi, Yun Nan, China, in 1971. She received the B.S. degree in automation, the M.S. degree in control theory and control engineering, and the Ph.D. degree in thermal power engineering from the North China Electric Power University, Baoding, China, in 1992, 2000, 2011, respectively.

From 1992 to 1997, she was an Assistant Engineer with Yunnan Thermal Power Construction Company, Ltd., and Baoding Sinosimu Technology Company, Ltd. Since 2000, she has been a Lecturer, and since 2011, has also been an Assistant Professor with the Automation Department, College of Electric Information Engineering, Hebei University. She is the author of three books and more than 40 articles. Her research interests include modeling and design of the photovoltaic power generation systems and energy storage, and the innovation and applications of active disturbance rejection control strategy.

● ● ●